Article
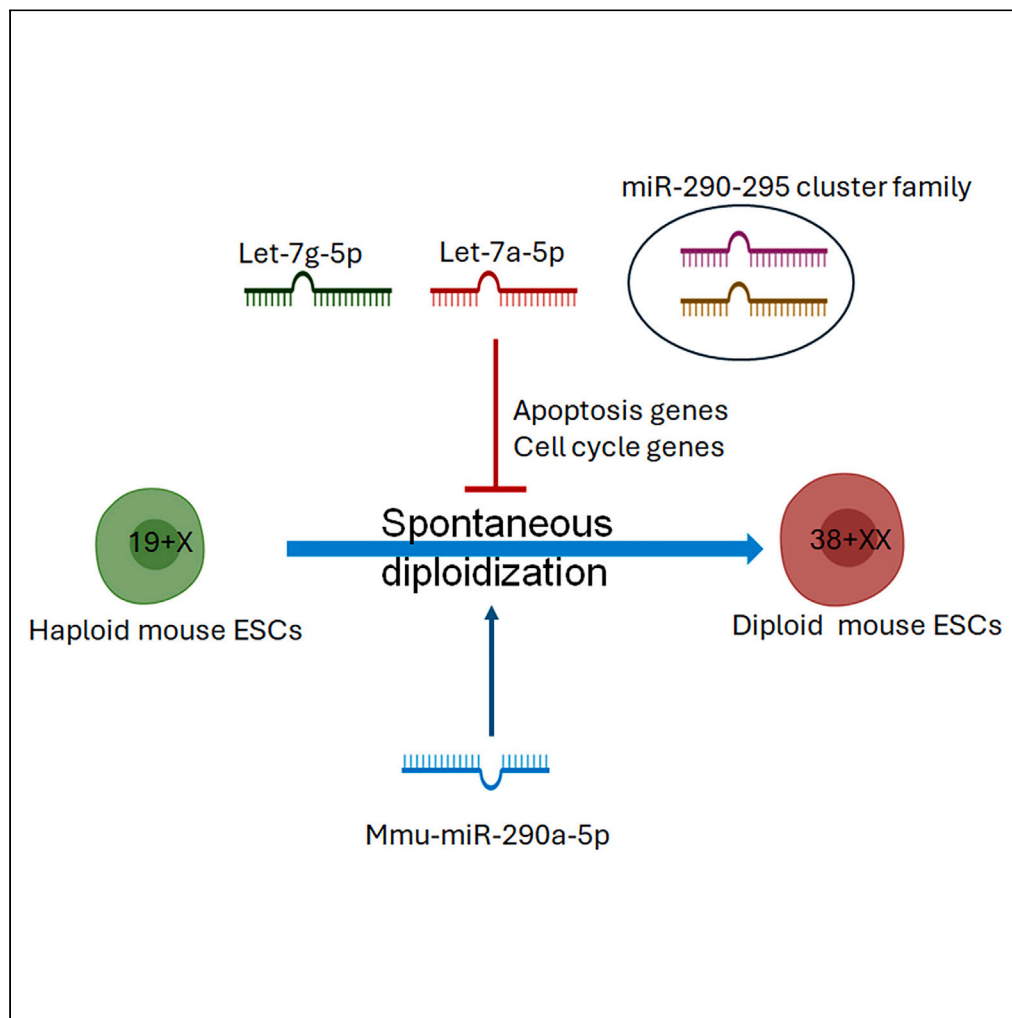
Overexpression of Let-7a mitigates diploidization in mouse androgenetic haploid embryonic stem cells

Wenteng He,
Hongming Tang,
Yuanyuan Li, ...,
Jiayu Chen,
Shaorong Gao,
Zhiming Han

gaoshaorong@tongji.edu.cn
(S.G.)
hanzm@ioz.ac.cn (Z.H.)

Highlights

The small RNA profiles of mAG-haESCs, R1, and mRS are distinct

mAG-haESCs have the unique microRNA profile

Many microRNAs involve in relevant KEGG pathways

Overexpression of Let-7a can mitigate diploidization in mAG-haESCs

Article

Overexpression of Let-7a mitigates diploidization in mouse androgenetic haploid embryonic stem cells

Wenteng He,[1,5] Hongming Tang,[1,5] Yuanyuan Li,[1] Mingzhu Wang,[1] Yuanyuan Li,[2] Jiayu Chen,[3] Shaorong Gao,[1,3,*] and Zhiming Han[2,4,6,*]

SUMMARY

Mouse androgenetic haploid embryonic stem cells (mAG-haESCs) can be utilized to uncover gene functions, especially those of genes with recessive effects, and to produce semicloned mice when injected into mature oocytes. However, mouse haploid cells undergo rapid diploidization during long-term culture _in vitro_ and subsequently lose the advantages of haploidy, and the factors that drive diploidization are poorly understood. In this study, we compared the small RNAs (sRNAs) of mAG-haESCs, normal embryonic stem cells (ESCs), and mouse round spermatids by high-throughput sequencing and identified distinct sRNA profiles. Several let-7 family members and miR-290-295 cluster microRNAs (miRNAs) were found significantly differentially transcribed. Knockdown and overexpression experiments showed that let-7a and let-7g suppress diploidization while miR-290a facilitates diploidization. Our study revealed the unique sRNA profile of mAG-haESCs and demonstrated that let-7a overexpression can mitigate diploidization in mAG-haESCs. These findings will help us to better understand mAG-haESCs and utilize them as tools in the future.

INTRODUCTION

Mouse androgenetic haploid embryonic stem cells (mAG-haESCs) are haploid cells derived from mouse androgenetic haploid blastocysts, which have only one set of genomes inherited from sperm.[1,2] mAG-haESCs can maintain pluripotency and propagate infinitely, similar to diploid embryonic stem cells (ESCs) (2n ESCs), under 2i culture conditions. Moreover, these cells are widely used for exploring gene loss-of-function phenotypes and in genetic screening due to their linearized genome and ability to efficiently produce semicloned mice by "fertilizing" mature oocytes in place of sperm.[3] At present, androgenetic and parthenogenetic haESC lines have been established in several mammalian species, including mice,[1] monkeys,[4] rats,[5] and humans.[6,7]

mAG-haESCs are prone to rapid diploidization in long-term _in vitro_ culture, resulting in androgenetic diploid ESCs with the loss of the advantages of haploidy. Diploidization occurs in haESCs through an irregular cell cycle with mitotic slippage, a process in which cells re-enter G1 phase without undergoing chromatid sister separation or cytokinesis.[8,9] There are three possible outcomes after such diploidization: first, normal proliferation after regular division, in which haploidy is maintained; second, haploid cells undergo diploidization and do not divide, becoming diploid cells; and third, after a failed prolonged M phase mitotic arrest leading to mitotic catastrophe (MC). Several ways to mitigate diploidization have been explored, including the addition of small molecular inhibitors (PD166285, Y-27632, and RO-3306),[9,10] suppression or overexpression (OE) of cell cycle-related genes (Dnmt3b and Aurora B),[8,11] and depletion of apoptosis-related genes (_p53_).[12] However, the effectiveness of these approaches was limited, and the mechanism that regulates diploidization is still unclear.

Noncoding RNAs (ncRNAs) are endogenous RNAs that do not encode proteins; they can be divided into long ncRNAs ($\geq$ 200 nt) and small ncRNAs (sncRNAs, 20–200 nt) according to their lengths. Based on their biogenesis and functions, sncRNAs are categorized as microRNAs (miRNAs), endogenous small interfering RNAs (endo-siRNAs), P-element induced wimpy testis (PIWI)-interacting RNAs (piRNAs), transfer RNAs (tRNAs), small nuclear RNAs (snRNAs), small nucleolar RNAs (snoRNAs), tRNA-derived small RNAs (tsRNAs), and other short RNAs. Among them, miRNAs (21–24 nt) are single-stranded short-chain RNAs that are involved in a variety of cell processes, including development, differentiation, proliferation, and apoptosis.[13] miRNAs mediate gene silencing post-transcriptionally by forming a translation repression

A Outgowth → AG-ESCs → FACS sorting → AG-haESCs

Cell lines
**A129-6, A129-7, A129-8, A129-10
A129-11, A129-15, A129-16,A129-17
A129-18, A129-19**

B A129-2 R1

C 4 weeks / 8 weeks

D Annotation of Total reads

- Known_miRNA
- Repeat
- snoRNA
- snRNA
- tRNA
- rRNA
- novel_miRNA
- Exon:+
- Exon:-
- intron:+
- intron:-
- other RNA

E Small RNA Length distribution

- mAG-haESCS
- R1
- mRS

F A129-2 / R1 / mRS

Figure 1. sRNA signature read analysis of mAG-haESCs, R1, and mRS

(A) Representative morphology of mouse androgenetic outgrowths and ES cells, as well as the 1n ratio of the first and second FACS sorting charts and 10 mAG-haESC lines. Scale bar, 100 μm.

(B) Representative images and FACS charts of A129-2 (mAG-haESCs) and R1 (2n ESCs). Scale bar, 100 μm.

(C) FACS charts of germ cells from 4- or 8-week-old mice and representative images of mouse round spermatids (mRSs). Scale bar, 100 μm.

(D) sRNA classification of all samples. The horizontal axis shows the percentage of total reads.

(E) Statistical analysis of the sRNA profiles of mAG-haESCs, R1, and mRS. Data are shown as the mean ± SEM.

(F) Representative length distribution statistics of the total sRNA fragments obtained from A129-2 (mAG-haESCs), R1, and mRS. The horizontal axis shows the reads length, and the vertical axis shows the proportion of reads of this length.

complex, which inhibits target gene function by binding to the 3′ untranslated region (3′UTR) of the mRNAs of its target genes. The miRNA-induced silencing complex (miRISC) subsequently promotes protein translation inhibition or degradation of target mRNAs.[14,15] miRNAs involved in the regulation of mouse early embryonic development, such as miR-675, modulate the growth of the placenta in late gestation.[16] Knockout of the cleavage enzymes that produce miRNAs, the ribonuclease III enzymes Dicer[17] and Drosha,[18] both of which have been demonstrated to play important roles in mouse cells and embryos, is embryonic lethal. However, the roles of miRNAs in mouse haploid cells have not been explored.

Mouse germ cells are derived from primordial germ cells (PGCs), which differentiate from epiblasts at E6.25.[19] Through propagation by mitosis and two rounds of meiosis in the testis, PGCs differentiate into round spermatids. Then it goes through spermatogenesis in the seminiferous tubules including elongating spermatids and elongated spermatids as well as round spermatids, which progress to mature spermatozoa after the loss of the cytoplasm. These processes involve complex molecular dynamics. For example, the spermatogenesis-related mRNAs are synthesized in mouse round spermatids (mRSs), but not in elongated spermatids or mature spermatozoa, and histone proteins are replaced by protamine. Round spermatids are the *in vivo* counterparts of *in vitro*-derived haploid cells and thus were used as a haploid cell control in this study.

To investigate the mechanism of diploidization in mAG-haESCs, we first compared the sRNA profiles of mAG-haESCs, normal 2n ESCs (R1), and mRS with the same genetic background through high-throughput sequencing. We characterized the unique miRNA profile of mAG-haESCs and identified many miRNAs involved in relevant Kyoto Encyclopedia of Genes and Genomes (KEGG) pathways. We further explored the functions of key miRNAs by modulating their expression and demonstrated that the OE of let-7a can mitigate diploidization in mAG-haESCs. In this study, we mapped the sRNAs profile of mAG-haESCs for the first time and proved that miRNAs participate in regulating diploidization in mAG-haESCs.

RESULTS

mAG-haESCs, mESCs, and mRS cells with the same genetic background

We uniformly selected Sv129 mouse-derived mAG-haESCs, normal 2n mESCs (R1), and mRS cells to exclude variation caused by differences in genetic background. First, we expanded the set of Sv129-derived mAG-haESC lines, establishing 10 new mAG-haESC cell lines from 25 androgenetic (AG) blastocysts which were developed from 224 reconstructed haploid embryos by injecting a single sperm head into enucleated oocyte. Then, we randomly selected 3 cell lines (A129-2, A129-6, and A129-17) as representatives for this study to characterize the traits of sRNAs in mAG-haESCs (Figures 1A and 1B). R1 was used as the diploid cell control for cultured mESCs *in vitro*, and mRS was used as a haploid cell control *in vivo*. Then, mRS from seminiferous tubules of 4- or 8-week-old Sv129 male mice were analyzed by fluorescence-activated cell sorting (FACS) after staining with Hoechst 33342 *in vitro*. According to the differences in germ cell size and DNA content, the testes germ cells were clearly divided into 4 groups, namely, primary spermatocytes, secondary spermatocytes, early round spermatids, and elongated spermatids, which were clearly arranged from top to bottom (Figure 1C). Among these cells, elongating and elongated spermatids have fewer RNAs, and their histones are gradually replaced with protamine; therefore, they are classified as gametes. The intrinsic morphology of these cells is different from that of haploid mRS cells. These characteristics indicate that the epigenetic signature of these cells could be quite different from that of mAG-haESCs. Therefore, round spermatids at an earlier stage were collected to avoid potential interference from elongating and elongated spermatids. Because spermatogenesis in mice occurs in waves beginning a few days after birth, the first wave of round spermatids begins to be produced at approximately 4 weeks after birth, and no elongating or elongated spermatids are produced at this point. Therefore, we used mRS cells from 4-week-old male Sv129 mice. Therefore, we established a flow cytometric sorting collection system for mRS and mAG-haESCs. We collected 3~5×10⁶ cells with 2 or 3 independent replicates for each sample (mAG-haESCs, R1, mRS), and at least 10 million clean mapped reads were obtained for each sample after sRNA sequencing.

The sRNA type (indicated by unique reads) and quantity (indicated by total reads) were screened based on length range analysis of clean reads, and then the length distribution of the sRNAs was evaluated. Each species-specific small ncRNA type, including rRNA, tRNA, snRNA, and snoRNA, was measured (Figure 1D). We next analyzed the length distribution of the sRNAs to determine the sRNA types. Our results demonstrated that the lengths of sRNAs in mAG-haESCs were mainly concentrated at 21–24 nt (64.48% ± 2.41% of the total reads) and 26–32 nt (14.99% ± 3.61% of the total reads); R1 sRNAs were mainly concentrated at 21–24 nt (61% ± 6.32%) and 26–32 nt (18.63% ± 3.52%), while mRS sRNAs were mainly concentrated at 26–32 nt (92.77% ± 0.36%) and 21–24 nt (accounting for 3.16% ± 0.25%) (Figures 1E and 1F). These results showed that the sRNAs in mAG-haESCs and R1 were mainly miRNAs with a small amount of piRNAs, while
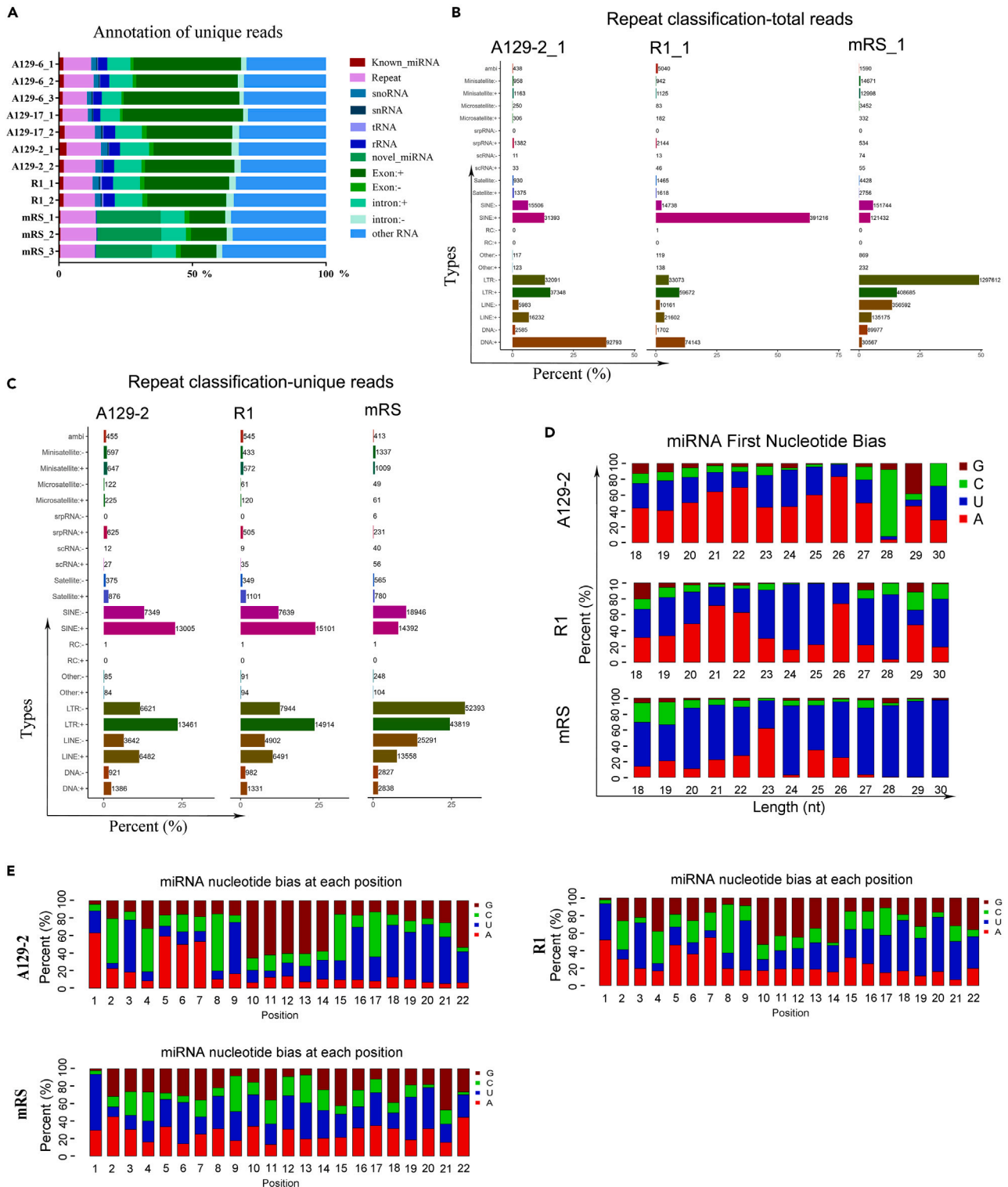
Figure 2. sRNA base profiles of mAG-haESCs, R1, and mRS

(A) sRNA classification of all samples. The horizontal axis shows the percentage of unique reads.

(B) Representative percentages of repeat classification based on total reads for A129-2, R1, and mRS. The horizontal axis shows the percentage of total reads. The vertical axis shows the type of repeat.

Figure 2. Continued

(C) Representative percentages of repeat classification based on unique reads of A129-2 (mAG-haESCs), R1, and mRS. The horizontal axis shows the percentage of unique reads.

(D) The first base preference of known miRNAs 18–30 nt in length. The abscissa is the miRNA length, and the ordinate is the percentage of A/U/C/G bases in the first position in the miRNAs of this length.

(E) The base preference of each base position in known miRNAs. The horizontal axis shows the miRNA base position, and the vertical axis shows the percentage of A/U/C/G bases in the miRNA at this position.

those in mRS were mainly piRNAs with fewer miRNAs. In addition, mAG-haESCs contained fewer piRNAs than R1 (14.99 vs. 18.63, Figure 1E), which is consistent with the unique piRNA metabolic process pathway of mAG-haESCs.

Unique base profile of sRNAs in mAG-haESCs

Annotation of the total reads indicated that miRNAs were more enriched in mouse pluripotent ESCs (mPESCs, including mAG-haESCs and R1) than in mRS sRNAs (Figures 1E and 1F). Further statistics on unique reads showed that, in A129-2, the known miRNAs accounted for 1.46% of reads, and newly discovered miRNAs accounted for 0.03%; in R1, the known miRNAs accounted for 1.32% of reads, and novel miRNAs accounted for 0.02%; and in mRS, the known miRNAs accounted for 0.21% of reads, and novel miRNAs accounted for 0% (Figure 2A). Among the miRNAs, 11.81% and 10.97% of the total sRNAs in A129-2 and R1, respectively, originated from repeat regions. Furthermore, most repeat located RNAs were distributed on transposons such as short interspersed nuclear elements (SINEs), long interspersed nuclear elements (LINEs), and long terminal repeats (LTRs) in mPESCs. However, in mRS, 13.27% of total sRNAs were located in repeat regions, mainly LTRs, and only a small proportion were in SINEs and LINEs compared to the situation in mPESCs (Figures 2B and 2C). These data indicated that the sRNAs in mRS more originated from LTRs retrotransposons, while the sRNAs in mPESCs more originated from non-LTR retrotransposons.

We next sought to explain what the bias in different cell types is expected to reveal about those cells as it relates to the mechanism of diploidization. We found that the first position of 18–27 nt sRNAs in mAG-haESCs was predominantly A; however, in mRS, it was predominantly U, especially the first base of 28–30 nt sRNAs. The first base of R1 sRNAs showed no preference between A and U (Figure 2D). In addition, base distribution analysis of known miRNA sites indicated that mAG-haESCs have obvious A bias at the 1st ($\geq$60%) and 5th–7th bases (approximately 60%), the 10th–14th ($\geq$60%) bases have a G bias, and the 18th–21st bases tend to be U (approximately 60%), while, in mRS, the bases at these positions have no obvious bias, with the bases A/T/C/G basically evenly distributed; the base bias at each position of R1 is similar to that of AG-haESCs, but less extreme (Figure 2E).

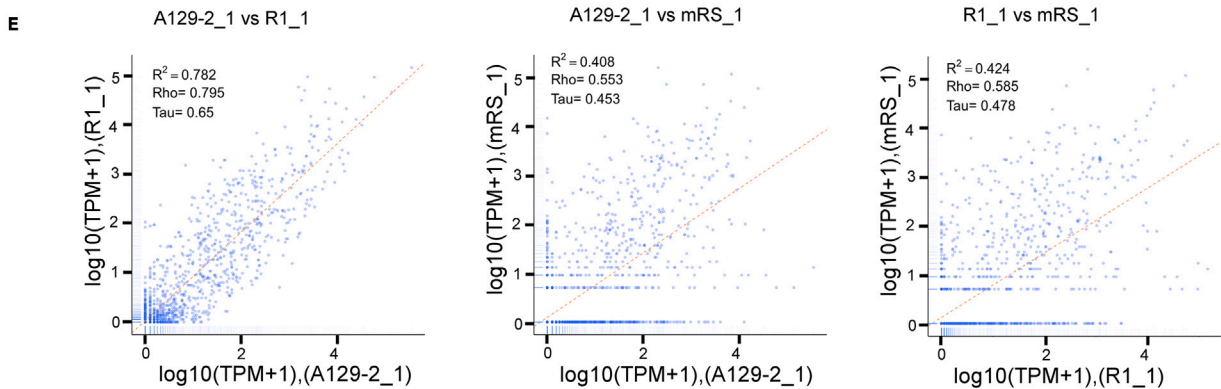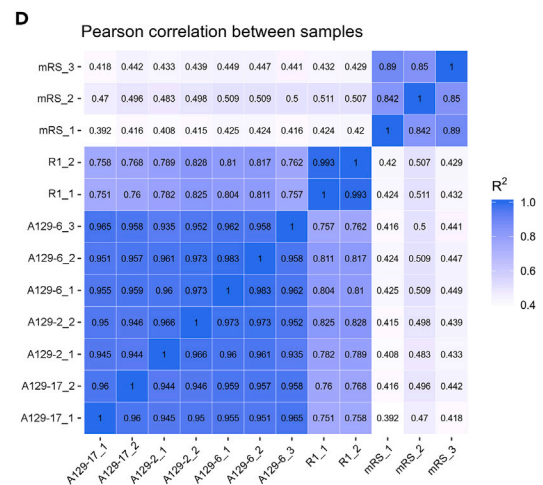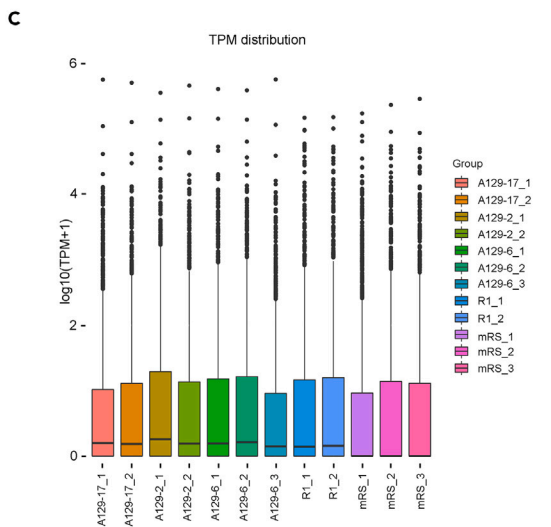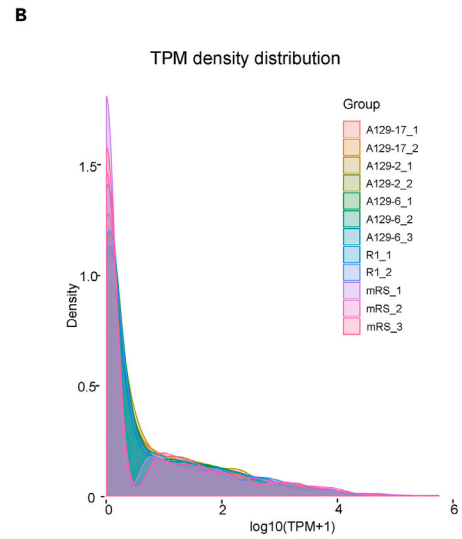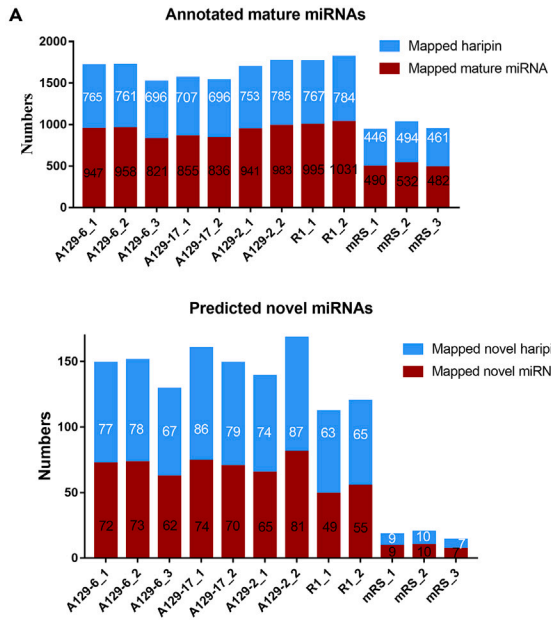Taken together, these results indicated that we obtained a high-quality sRNA profile of mAG-haESCs. mAG-haESCs have a unique sRNA signature compared to R1 and mRS in terms of the length distribution, sRNA type distribution, first-base distribution, and base position preference of known miRNAs.

miRNA expression profile of mAG-haESCs

We next aimed to uncover the expression profile patterns of the remaining mature miRNAs that matched with known miRNAs. We found that mPESCs contained approximately 1,800 miRNAs, while approximately 1,000 miRNAs from mRS were mapped (Figure 3A). The transcripts per million (TPM) density distribution, which represents the global gene expression pattern of the sample, indicated that mAG-haESCs (7 samples), R1 (2 samples), and mRS (3 samples) had different expression patterns; in short, mPESCs have similar expression patterns that are completely different from those of mRS (Figures 3B and 3C). The correlation of gene expression levels was analyzed between samples. The Pearson correlation coefficient showed high reproducibility within each group (mPESC group correlation coefficient >0.9, mRS group correlation coefficient >0.8) and low correlation coefficients between different groups, indicating that the sequencing data were reliable. Additionally, the miRNA expression pattern of mAG-haESCs was similar to that of R1 but quite different from that of mRS (Figure 3D). Furthermore, the miRNA scatterplot showed that A129-2 had a high correlation with R1 (R2 = 0.782) and a low correlation with mRS (R2 = 0.408). This low correlation may be due to the difference in cell types between mPESCs and mRS and R1, as mRS also had a low correlation with R1 (R2 = 0.424, Figure 3E).

Differential miRNA analysis of the overall hierarchical cluster analysis showed that the differential miRNA expression patterns of mAG-haESCs were different from those of R1 and mRS (Figure 4A). Furthermore, the differentially expressed miRNAs were compared through a Venn diagram. A total of 370 miRNAs were found to be shared among all mAG-haESCs and distinct in R1, and 382 miRNAs were found to be shared among all mAG-haESCs and distinct in mRS (Figure 4B). The volcano map shows the overall distribution of differential miRNAs (fold change) and the corrected significance level (padj/q value). Compared with mRS, A129-2 had 265 significantly upregulated miRNAs and 169 significantly downregulated miRNAs (Figures 4C and 4D). In addition, A129-2 had 211 significantly upregulated and 246 significantly downregulated miRNAs compared to R1 (Figures 4C and 4D). Moreover, according to the analysis by cell type, we found that R1 had 275 significantly upregulated and 182 significantly downregulated miRNAs compared with mRS (Figures 4C and 4D). In particular, several miRNAs of the let-7 family and miR-290-295 cluster families were significantly differentially expressed (Figure 4D).

The candidate target genes of the differentially expressed miRNAs between mAG-haESCs and R1 were analyzed via KEGG enrichment pathway analysis, which yielded a rich factor, Q value, and the number of genes enriched in the pathway. Compared with mRS, A129-2 exhibited significant differences in many KEGG signaling pathways, including the Wnt signaling pathway, Ras

A

Annotated mature miRNAs

Predicted novel miRNAs

B

TPM density distribution

C

TPM distribution

D

Pearson correlation between samples

E

A129-2_1 vs R1_1

$R^2 = 0.782$
Rho= 0.795
Tau= 0.65

A129-2_1 vs mRS_1

$R^2 = 0.408$
Rho= 0.553
Tau= 0.453

R1_1 vs mRS_1

$R^2 = 0.424$
Rho= 0.585
Tau= 0.478

Figure 3. miRNA profiles of mAG-haESCs, R1, and mRS

(A) Statistics of annotated known mature miRNAs and predicted novel miRNAs in mAG-haESCs, R1, and mRS.

(B) TPM density distribution map. The abscissa is the $\log_{10}(TPM+1)$ value of the miRNA, and the ordinate is the corresponding density.

(C) The TPM pattern of each sample. The vertical axis indicates density, corresponding to $\log_{10}(TPM+1)$.

(D) The correlation of miRNA expression levels among sample replicates.

(E) Representative correlation analysis between the indicated sample replicates.

signaling pathway, and mitogen-activated protein kinase (MAPK) signaling pathway, which regulate cell proliferation and apoptosis; metabolic pathways and the PI3K-Akt pathway, which are related to metabolism and apoptosis signaling; and signaling pathways regulating pluripotency in stem cells, which represented the differences in cell types between ESCs and round spermatids (Figure 4E).

Compared with R1, A129-2 exhibited significant differences in many KEGG signaling pathways, including the Wnt signaling pathway, Ras signaling pathway, MAPK signaling pathway, mammalian target of rapamycin (mTOR) signaling pathway, and insulin signaling pathway. Among these pathways, the Ras signaling pathway is involved in cell proliferation, apoptosis, and cytoskeletal movement. The Wnt signaling pathway is involved in cell proliferation and asymmetric division, and the MAPK signaling pathway is involved in cell proliferation, differentiation, division, and apoptosis. These pathways correspond to the diploidization of haploid cells and are consistent with the cellular features of mAG-haESCs, indicating that our miRNA data accurately reflect the characteristics of the sample. The results also illustrated that different miRNAs play important roles in various types of cellular processes in mAG-haESCs (Figure 4F).

Taken together, the results of the KEGG pathway analysis of the candidate target genes of the differentially expressed miRNAs indicate that mAG-haESCs have a unique miRNA expression profile with distinct impacts on the physiological processes of cell proliferation, apoptosis, and metabolism. Moreover, these differentially transcribed miRNAs play important regulatory roles in these pathways and may affect them by negatively regulating the expression of their target genes.

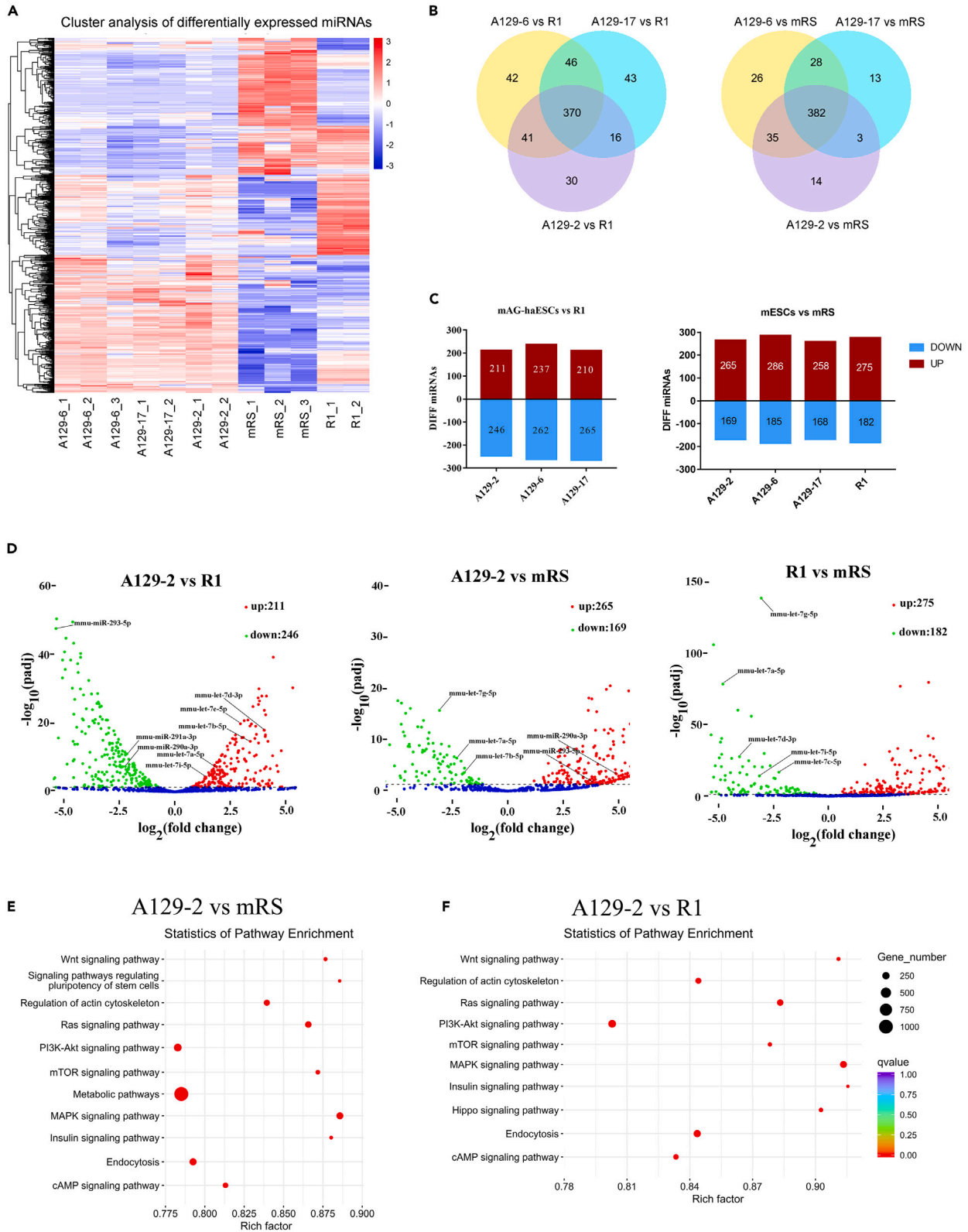### Inhibition of the Let-7 family accelerates mAG-haESC diploidization

Many miRNAs involved in KEGG pathways related to cell proliferation, division, apoptosis, and other pathways were identified. To explore the roles of these miRNAs in various physiological processes, we attempted to modulate the expression of several miRNAs. In mice, let-7a and let-7g, which belong to the let-7 family, were expressed at significantly higher levels in mAG-haESCs than in R1 but at significantly lower levels than in mRS (Figure 5A). Let-7a/7g/7i negatively regulate the expression of Aurora B,[20] and Aurora B OE can delay the diploidization rate of haploid cells.[8] Therefore, we hypothesized that knocking down let-7a/g/i to promote Aurora B expression could affect the rate of diploidization. Recently, miRNA sponge technology has become the most common and effective way to knock down miRNAs; the miRNA sponges are competitive inhibitory sRNAs based on the seed sequence (from 2 to 8 nt at the 5′ end) of the miRNA family that compete for the targeted binding sequence. As a result, the binding of the target gene sequence by the miRNA is inhibited. The seed sequence of the let-7 family is GAGGTA (miRbase data), which we used in the sponge fragment that we designed to block the function of the entire let-7 family.

The let-7 sponge plasmid was stably introduced into the A129-2 cell line by lentivirus, and the cells were treated with puromycin for 14 days. Then, the reconstructed cell lines (A129-2-let-7 sponge) were induced with doxycycline (Dox) to express the let-7 sponge fragment. Quantitative real-time PCR (real-time qPCR) confirmed that the let-7 sponge fragment was overexpressed 3-fold in the A129-2-let-7 sponge (+Dox) group compared with the A129-2-let-7 sponge (-Dox) group (Figure 5B). Unexpectedly, we found through FACS analysis that the diploidization rate of the A129-2-let-7 sponge (+Dox 3 days) group was accelerated compared with that of the A129-2-let-7 sponge (-Dox) group at day 9 after last FACS sorting. Meanwhile, there was no difference between the blank control (BC) group A129-2-BC (+Dox) and A129-2-BC (-Dox) (Figures 5C and 5D). In the 9-day Dox treatment group, the diploidization rate was further accelerated compared to that of the 3-day Dox treatment group (Figure 5C). We speculate that this may be because the sRNA sponge fragments are rapidly degraded in cells, and continuous Dox treatment maintains the sRNA sponge fragment expression level. Therefore, we extended the Dox induction to longer cell culture times and observed that A129-2-let-7 sponge (+Dox) continuously reduced the proportion of haploid cells compared with the corresponding -Dox group (Figure 5E). Due to most target genes of differentially transcribed miRNAs in mAG-haESCs being involved in KEGG pathways of apoptosis and cell proliferation (Figures 4E and 4F), we hypothesized that changes in the diploidization rate after let-7 sponging could occur through the regulation of apoptosis and cell proliferation genes. As expected, detection of apoptosis-related gene expression by real-time qPCR revealed that genes involved in promoting apoptosis, including *Survivin*, *Hras*, *p53*, *Bax*, *Chek2*, *Caspase2*, and *Caspase3*, were significantly upregulated (Figure 5F). Knockout or low expression of the *p53* and *Chek2* genes has been reported to slow the diploidization rate.[11,12] Let-7a is downstream of the *p53* response pathway, and a decrease in let-7a expression promotes the expression of cell death or apoptosis genes.[21] Therefore, the acceleration of mAG-haESC diploidization through the inhibition of let-7 family function may occur through the regulation of the apoptosis pathway, resulting in MC.

Reduction of diploidization in mAG-haESCs induced by several miRNAs

Since inhibiting the function of the let-7 family accelerated the diploidization rate of haploid cells, we wondered whether OE of let-7 family members could reduce the diploidization rate. First, mmu-let-7a-5p mimics and inhibitors were synthesized and transiently transfected into A129-2 cells via Lipo2000. The mimic control (double-stranded) and inhibitor negative control (single-stranded) were transfected independently. The diploidization rate of haploid cells was detected at 96 h after transfection. As expected, we found that the diploidization rate of haploid cells in the let-7a-5p mimic group was significantly reduced compared with that of the mimic control group. Conversely, the

A Cluster analysis of differentially expressed miRNAs

B

C

mAG-haESCs vs R1

mESCs vs mRS

D

A129-2 vs R1

A129-2 vs mRS

R1 vs mRS

E A129-2 vs mRS
Statistics of Pathway Enrichment

F A129-2 vs R1
Statistics of Pathway Enrichment

Figure 4. miRNA transcription patterns and differentially transcribed miRNA analysis

(A) Overall hierarchical clustering diagram of differential miRNAs clustered by $\log_{10}$(TPM+1) value. Red indicates high miRNA expression, and blue indicates low miRNA expression.

(B) Venn diagram of differentially expressed miRNAs. The overlapping circles indicate the number of differentially expressed miRNAs shared between samples.

(C) Differentially transcribed miRNAs (up- and downregulated) in the indicated sample compared to R1 and mRS. The vertical axis shows the number of differentially transcribed miRNAs.

(D) Volcano plot of differentially expressed miRNAs. The blue dots represent miRNAs with no significant difference, the red dots represent significantly upregulated miRNAs, and the green dots represent significantly downregulated miRNAs.

(E) Representative KEGG enrichment scatterplot of differential miRNA candidate target genes between A129-2 and mRS.

(F) Representative KEGG enrichment scatterplot of differential miRNA candidate target genes between A129-2 and R1.

diploidization rate of haploid cells in the let-7a-5p inhibitor group was significantly accelerated compared with that of the inhibitor negative control (NC) group (Figure 6A). These results indicate that OE of mmu-let-7a-5p can reduce the diploidization rate of mAG-haESCs, while inhibition of let-7a-5p accelerates the diploidization rate. To further confirm these results and constitutively continuously overexpress let-7a-5p, the let-7a fragment was cloned instead of the let-7a sponge fragment into the same plasmid and stably introduced into A129-2 cells. The sequence and structure of mmu-let-7a-5p used for functional verification are presented in Figure 6B. After drug screening using puromycin, let-7a was overexpressed by continuous induction with Dox. The diploidization rate of haploid cells in the A129-2-let-7a OE cell line was detected at different cell culture time points. The results showed that the percentage of haploid cells in the A129-2-let-7a OE (+Dox) group was significantly higher than that in the A129-2-let-7a OE (-Dox) group at each culture time point after Dox treatment (Figure 6B), consistent with the results obtained with the mmu-let-7a-5p mimics. Next, to understand the mechanism underlying these results, real-time qPCR was performed to investigate the expression of 60 genes related to cell-cycle regulation and/or apoptosis. We found that the expression of genes related to apoptosis, including *Survivin*, *Hras*, *p16* (also known as *Ink4a/CDKN2A*), and *Caspase1*, was significantly downregulated in A129-2-let-7a OE (+Dox) cells (Figure 6C). Conversely, the expression level changes of these genes were negatively correlated with those in the let-7a sponge group, in which the diploidization rate was increased (Figure 5F). In addition, we found significant changes in the expression level of genes that regulate cell proliferation and the cell cycle, including *Rb*, *Nupr1*, *Ccnd1*, *CDK6*, *Cdc20*, and *Myc* (Figure 6D). Taken together, the aforementioned results indicate that let-7a mitigates the diploidization rate by regulating the expression of cell cycle- and apoptosis-related genes during diploidization in mAG-haESCs.

In mouse ESCs, the mmu-290-295 cluster family accounts for 60% of total miRNAs.[22] Further experiments were performed to test the functions of two other miRNAs (mmu-let-7g-5p and mmu-290-295 cluster family) that were significantly expressed in mAG-haESCs. The sequences and structures of mmu-let-7g-5p and mmu-miR-290a-5p used for functional verification are presented in Figure 6E. The mmu-let-7g-5p and mmu-miR-290a-5p mimics and controls were synthesized and transfected into A129-2 cells. As expected, compared to the corresponding control groups, mmu-let-7g-5p mimics reduced the diploidization rate, while mmu-miR-290a-5p mimics significantly accelerated the diploidization rate (Figure 6F). Furthermore, since several of the rest miRNA members of miR-290-295 cluster family were differentially transcribed in mAG-haESCs (Figure 4D), we wondered whether the function of the whole miR-290-295 cluster family was involved in diploidization rate. Therefore, the whole miR-290-295 cluster family fragment (2.8 kb) was stably introduced into A129-2 cells by plasmid construction, and we found that the diploidization rate of haploid cells decreased significantly at different culture times under continuous Dox treatment (Figure 6G). Similarly, the expression levels of the apoptosis-related genes *Survivin* and *p16* were significantly downregulated, while no significant changes were observed in the remaining apoptosis-related genes (Figure 6H). These findings suggest that the entire miR-290-295 cluster family may act through other apoptosis regulatory pathways different from those activated by let-7a to reduce the diploidization rate of A129-2 cells.

DISCUSSION

sRNAs are short ncRNAs, including miRNAs, siRNAs, and piRNAs, that play important roles in multiple cell biological processes. In this study, we mapped the sRNAs profile of mAG-haESCs for the first time and evaluated the functions of several miRNAs. The sRNAs in mPESCs were enriched mainly in miRNAs and contained only a small number of piRNAs, while mRS had abundant piRNAs but fewer miRNAs. In addition, mAG-haESCs contained fewer piRNAs than R1. The global miRNA expression pattern of mAG-haESCs is similar to that of R1 but quite different from that of mRS. Furthermore, the sRNAs of mAG-haESCs have obvious preferences in the base distributions at specific positions, including the first base, which are distinct from the preferences in R1 and mRS. Our findings show that multiple differentially expressed miRNAs play an important role in the diploidization of mAG-haESCs. These differentially expressed miRNAs might modulate the diploidization of mAG-haESCs through different regulatory pathways.

Lethal-7 (let-7) is one of two early miRNAs discovered in *Caenorhabditis elegans* (*C. elegans*) and is a major regulator of growth.[23] The let-7 family and miR-290-295 cluster are enriched in somatic and pluripotent stem cells, respectively. Several miRNAs were differentially transcribed in mAG-haESCs. Let-7a-5p, let-7f-5p, let-7g-5p, and let-7i-5p were highly transcribed in mAG-haESCs and mRS. Inhibition of let-7 family function with a sponge strategy resulted in an accelerated diploidization rate. Under the pressure of endoduplication, haploid cells undergo MC, which involves the upregulation of *p53*, the apoptosis-related genes *Survivin*, *Hras*, and *Bax*, and the mitotic checkpoint gene *Chek2*. As reported previously, Let-7 miRNA can regulate p53 and K-ras expression in colorectal cancer cells.[24] In addition, let-7 family members target the expression of proteins involved in cell proliferation (such as Ras)[25] and cell-cycle regulatory proteins (such as Cdc25A and cyclin D1), which can help suppress tumor growth.[26,27] After chemotherapy, let-7a expression in mouse ovaries decreased significantly. The transfer of let-7a
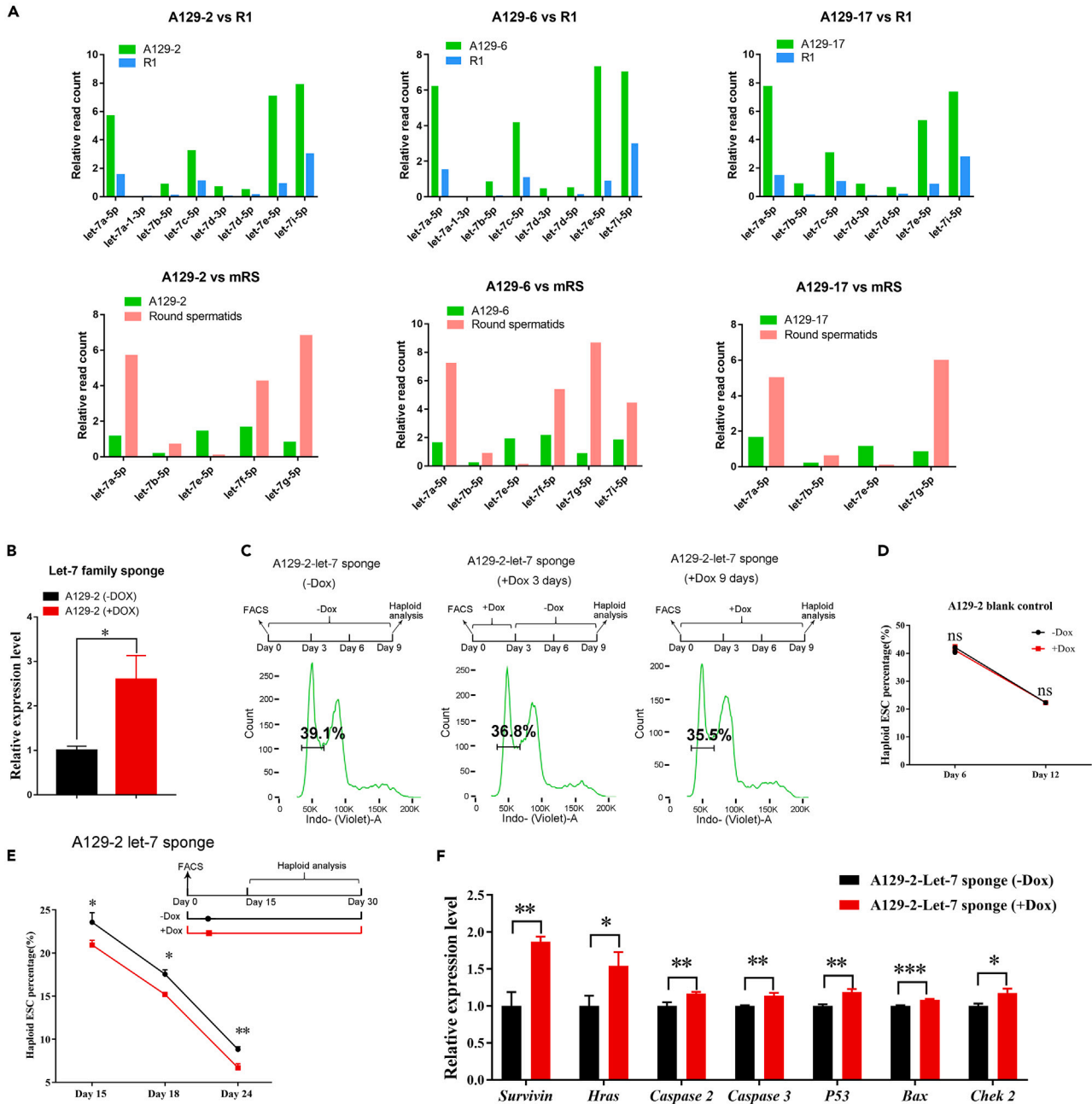
Figure 5. Repression of the let-7 family accelerates the mAG-haESC diploidization rate

(A) Relative read counts of let-7 family miRNA transcripts in mAG-haESCs, R1, and mRS.
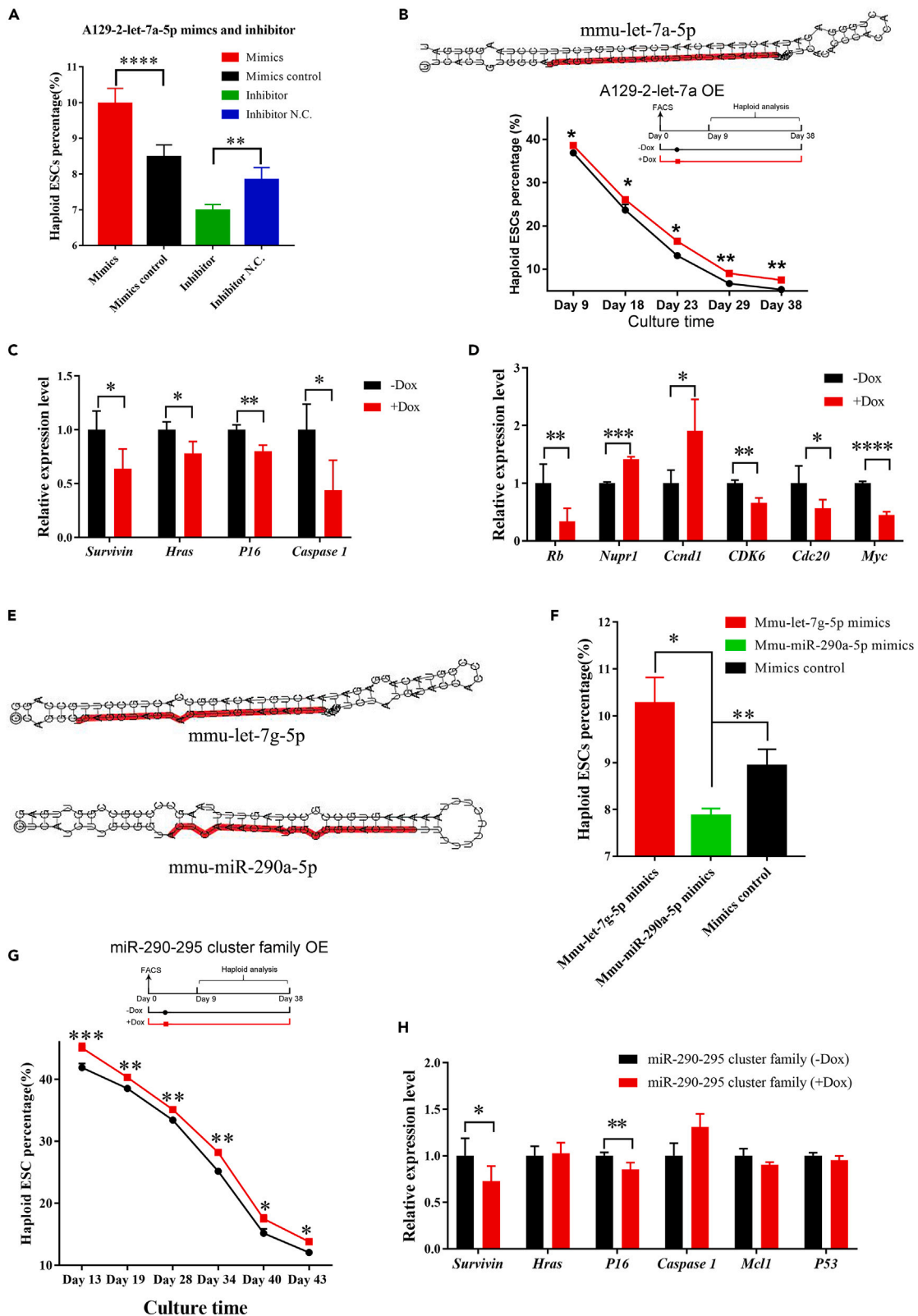
(B) Relative expression level of let-7 sponge fragment after Dox induction.

(C) Representative diploidization analysis in the indicated A129-2-let-7 sponge +/− Dox AG-haESCs.

(D) Diploidization analysis in the indicated A129-2 blank control group +/− Dox AG-haESCs. The vertical axis shows the percentage of haploid cells, and the horizontal axis shows the corresponding culture time ($n = 3$ independent experiments).

(E) Diploidization analysis of A129-2-let-7 sponge +/− Dox AG-haESCs in long-term culture ($n = 3$ independent experiments).

(F) Relative expression levels of cell cycle- and apoptosis-related genes in the indicated A129-2-let-7 sponge +/− Dox AG-haESCs. The expression level was normalized to *Gapdh* expression and compared with that observed in A129-2-let-7 sponge (-Dox) AG-haESCs ($n = 3$ independent experiments). Data in (B) and (D)–(F) are presented as the mean ± SEM. $*p < 0.05$; $**p < 0.01$; $***p < 0.001$ by Student's t test for comparison. ns, not significantly different.

A A129-2-let-7a-5p mimcs and inhibitor

B mmu-let-7a-5p

A129-2-let-7a OE

C

D

E mmu-let-7g-5p

mmu-miR-290a-5p

F

G miR-290-295 cluster family OE

H

Figure 6. Modulation of the diploidization rate in mAG-haESCs through the regulation of several miRNA transcripts

(A) Effects of let-7a-5p mimics and inhibitors on the diploidization rate in A129-2 cells. The vertical axis shows the percentage of haploid cells.

(B) Upper is the sequence and structure of mmu-let-7a-5p. Down is diploidization analysis in the indicated A129-2 let-7a-5p overexpression (OE) group +/− Dox AG-haESCs. The vertical axis shows the percentage of haploid cells, and the horizontal axis shows the corresponding culture time (n = 3 independent experiments).

(C) Relative expression of apoptosis-related genes determined by real-time qPCR in the indicated A129-2-let-7a overexpression group +/− Dox AG-haESCs. The expression level was normalized to *Gapdh* expression and compared with that observed in A129-2-let-7a-overexpressing (-Dox) AG-haESCs (n = 3 independent experiments).

(D) Relative expression of cell cycle-related genes determined by real-time qPCR in the indicated A129-2-let-7a overexpression group +/− Dox AG-haESCs. The expression level was normalized to *Gapdh* expression and compared with that observed in A129-2-let-7a-overexpressing (-Dox) AG-haESCs (n = 3 independent experiments).

(E) Sequences and structures of mmu-let-7g-5p (upper) and mmu-miR-290a-5p (lower).

(F) Effects of mmu-let-7g-5p mimics and mmu-mir-290a-5p mimics on the diploidization rate of A129-2 cells. The vertical axis shows the percentage of haploid cells.

(G) Diploidization analysis in the indicated A129-2-miR-290-295 cluster family overexpression group +/− Dox AG-haESCs. The vertical axis shows the percentage of haploid cells, and the horizontal axis shows the corresponding culture time (n = 3 independent experiments).

(H) Relative expression of cell cycle- and apoptosis-related genes in the indicated A129-2-miR-290-295 cluster family overexpression group +/− Dox AG-haESCs determined by real-time qPCR. The expression level was normalized to *Gapdh* expression and compared with that observed in A129-2-let-7a-overexpressing (-Dox) AG-haESCs (n = 3 independent experiments). Data in (A)–(D) and (F)–(H) are presented as the mean ± SEM. $*p < 0.05$; $**p < 0.01$; $***p < 0.001$; $****p < 0.0001$ by Student's t test for comparison.

mimics can inhibit the expression of cell death-related genes, such as the genes *Bax* and *FasL*, and chemotherapy-induced ovarian apoptosis.[28] Let-7a-5p mimics and let-7a OE can reduce the diploidization rate by improving haploid cell viability and cell-cycle regulation. Through let-7a OE, haploid cell viability was improved by repressing the expression of the apoptosis genes *Survivin*, *Hras*, *p16*, and *Caspase*. Accordingly, the cell-cycle genes *Rb*, *Nupr1*, *Ccnd1*, *CDK6*, and *Cdc20* were optimally regulated for haploid cell-cycle progression and proliferation.

In addition, let-7g-5p mimics reduced the diploidization rate, while miR-290a-5p mimics accelerated diploidization. Notably, the miR-290-295 cluster is transcribed primarily in mESCs, accounts for 60% of miRNAs in these cells, and plays a role in pluripotency maintenance; its expression decreases quickly when differentiation begins.[22,29] The miR-290-295 cluster maintains pluripotency by shortening the G1 phase and extending S phase. In addition, the regulation of S and G2 phase entry is mediated by the ATM/ATR-CHEK2-*p53* and Cyclin B1 pathways, respectively, to maintain pluripotency.[30,31] Moreover, the OE of the whole miR-290-295 family can reduce the diploidization rate by repressing *Survivin* and *p16*. Notably, *Survivin* acts simultaneously as a cell-cycle regulator and negative regulator of apoptotic cell death. Accordingly, repressing *p16* boosts cell-cycle progression from G1 to S phase, while upregulating *p16* expression results in cell-cycle delay from G1 to S phase by suppressing cyclin D-CDK4 kinase activation.[32] Furthermore, we identified *Survivin* and *p16* as two key genes involved in the cell death process during MC in haploid cells, in addition to the previously reported *p53*-involved cell apoptosis pathway.[12]

In summary, our study revealed the sRNA profile of mAG-haESCs and demonstrated that the OE of let-7a can mitigate diploidization in mAG-haESCs for the first time. However, we did not observe a cumulative effect of slowing diploidization as we reported previously in *Dnmt3b* OE.[11] This could be due to the rapid degradation of miRNAs inside the cell and limited capability to inhibit target gene function. sRNAs (miRNAs), which are involved in proliferation, apoptosis, differentiation, and cell-cycle regulation, play important roles in biological processes in mAG-haESCs, and their activities could offer new explanations for certain features inherent to haploid cells. Moreover, mAG-haESCs are a unique tool for revealing the biological functions of classic sRNAs in the future, including some functions that have been obscured in traditional research models. Given the diverse application potential of mAG-haESCs, these findings here on the functions and mechanisms of miRNAs provide a new approach to reduce the diploidization rate in mAG-haESCs, which will contribute to maintaining the haploid state of mAG-haESCs and making the advantages of haploid pluripotent stem cells for broad research and application prospects.

Limitations of the study

Although we mapped the sRNA profile of mAG-haESCs and proved that miRNAs participate in regulating diploidization in mAG-haESCs in this study, the mechanism of diploidization still needs to be further investigated. To further understand the function and mechanism of miR-NAs during the diploidization of mAG-haESCs, we should investigate the effect of the miRNA mimics and inhibitors on more cell lines from mice and other species as well in future studies.

STAR★METHODS

Detailed methods are provided in the online version of this paper and include the following:

- KEY RESOURCES TABLE
- RESOURCE AVAILABILITY
  - Lead contact
  - Materials availability
  - Data and code availability

- EXPERIMENTAL MODEL AND STUDY PARTICIPANT DETAILS
  - Mice
- METHOD DETAILS
  - Derivation and maintenance of mAG-haESCs
  - Collection of mRS, mAG-haESCs and R1 cells
  - sRNA extraction
  - sRNA library construction and sequencing
  - sRNA data analysis
  - Quality control of the sRNA sequencing data
  - Design and construction of miRNA sponges
  - Transfection of miRNA into mAG-haESCs
- QUANTIFICATION AND STATISTICAL ANALYSIS

AUTHOR CONTRIBUTIONS

W.H., J.C., S.G., and Z.H. conceived and designed this study. W.H. and H.T. conducted most of the experiments. Yuanyuan Li (author 3), M.W., and Yuanyuan Li (author 5) participated in FACS and plasmid construction. W.H., S.G., and Z.H. wrote the paper.

DECLARATION OF INTERESTS

The authors declare no competing interests.

REFERENCES

1. Li, W., Shuai, L., Wan, H., Dong, M., Wang, M., Sang, L., Feng, C., Luo, G.Z., Li, T., Li, X., et al. (2012). Androgenetic haploid embryonic stem cells produce live transgenic mice. Nature 490, 407–411.

2. Yang, H., Shi, L., Wang, B.-A., Liang, D., Zhong, C., Liu, W., Nie, Y., Liu, J., Zhao, J., Gao, X., et al. (2012). Generation of Genetically Modified Mice by Oocyte Injection of Androgenetic Haploid Embryonic Stem Cells. Cell 149, 605–617.

3. Zhong, C., Yin, Q., Xie, Z., Bai, M., Dong, R., Tang, W., Xing, Y.H., Zhang, H., Yang, S., Chen, L.L., et al. (2015). CRISPR-Cas9-Mediated Genetic Screening in Mice with Haploid Embryonic Stem Cells Carrying a Guide RNA Library. Cell Stem Cell 17, 221–232.

4. Yang, H., Liu, Z., Ma, Y., Zhong, C., Yin, Q., Zhou, C., Shi, L., Cai, Y., Zhao, H., Wang, H., et al. (2013). Generation of haploid embryonic stem cells from Macaca fascicularis monkey parthenotes. Cell Res. 23, 1187–1200.

5. Li, W., Li, X., Li, T., Jiang, M.G., Wan, H., Luo, G.Z., Feng, C., Cui, X., Teng, F., Yuan, Y., et al. (2014). Genetic modification and screening in rat using haploid embryonic stem cells. Cell Stem Cell 14, 404–414.

6. Sagi, I., Chia, G., Golan-Lev, T., Peretz, M., Weissbein, U., Sui, L., Sauer, M.V., Yanuka, O., Egli, D., and Benvenisty, N. (2016). Derivation and differentiation of haploid human embryonic stem cells. Nature 532, 107–111.

7. Zhong, C., Zhang, M., Yin, Q., Zhao, H., Wang, Y., Huang, S., Tao, W., Wu, K., Chen, Z.-J., and Li, J. (2016). Generation of human haploid embryonic stem cells from parthenogenic embryos obtained by microsurgical removal of male pronucleus. Cell Res. 26, 743–746.

8. Guo, A., Huang, S., Yu, J., Wang, H., Li, H., Pei, G., and Shen, L. (2017). Single-Cell Dynamic Analysis of Mitosis in Haploid Embryonic Stem Cells Shows the Prolonged Metaphase and Its Association with Self-diploidization. Stem Cell Rep. 8, 1124–1134.

9. He, Z.Q., Xia, B.L., Wang, Y.K., Li, J., Feng, G.H., Zhang, L.L., Li, Y.H., Wan, H.F., Li, T.D., Xu, K., et al. (2017). Generation of Mouse Haploid Somatic Cells by Small Molecules for Genome-wide Genetic Screening. Cell Rep. 20, 2227–2237.

10. Takahashi, S., Lee, J., Kohda, T., Matsuzawa, A., Kawasumi, M., Kanai-Azuma, M., Kaneko-Ishino, T., and Ishino, F. (2014). Induction of the G2/M transition stabilizes haploid embryonic stem cells. Development 141, 3842–3847.

11. He, W., Zhang, X., Zhang, Y., Zheng, W., Xiong, Z., Hu, X., Wang, M., Zhang, L., Zhao, K., Qiao, Z., et al. (2018). Reduced Self-Diploidization and Improved Survival of Semi-cloned Mice Produced from Androgenetic Haploid Embryonic Stem Cells

through Overexpression of Dnmt3b. Stem Cell Rep. 10, 477–493.

12. Olbrich, T., Mayor-Ruiz, C., Vega-Sendino, M., Gomez, C., Ortega, S., Ruiz, S., and Fernandez-Capetillo, O. (2017). A p53-dependent response limits the viability of mammalian haploid cells. Proc. Natl. Acad. Sci. USA 114, 9367–9372.

13. Tüfekci, K.U., Meuwissen, R.L.J., and Genç, S. (2014). The role of microRNAs in biological processes. Methods Mol. Biol. 1107, 15–31.

14. O'Brien, J., Hayder, H., Zayed, Y., and Peng, C. (2018). Overview of MicroRNA Biogenesis, Mechanisms of Actions, and Circulation. Front. Endocrinol. 9, 402.

15. Gebert, L.F.R., and MacRae, I.J. (2019). Regulation of microRNA function in animals. Nat. Rev. Mol. Cell Biol. 20, 21–37.

16. Keniry, A., Oxley, D., Monnier, P., Kyba, M., Dandolo, L., Smits, G., and Reik, W. (2012). The H19 lincRNA is a developmental reservoir of miR-675 that suppresses growth and Igf1r. Nat. Cell Biol. 14, 659–665.

17. Bernstein, E., Kim, S.Y., Carmell, M.A., Murchison, E.P., Alcorn, H., Li, M.Z., Mills, A.A., Elledge, S.J., Anderson, K.V., and Hannon, G.J. (2003). Dicer is essential for mouse development. Nat. Genet. 35, 215–217.

18. Chong, M.M.W., Zhang, G., Cheloufi, S., Neubert, T.A., Hannon, G.J., and Littman, D.R. (2010). Canonical and alternate functions

of the microRNA biogenesis machinery. Genes Dev. *24*, 1951–1960.

19. Saitou, M., and Hayashi, K. (2021). Mammalian *in vitro* gametogenesis. Science *374*, eaaz6830.

20. Yu, J.J., Pi, W.S., Cao, Y., Peng, A.F., Cao, Z.Y., Liu, J.M., Huang, S.H., Liu, Z.L., and Zhang, W. (2018). Let-7a inhibits osteosarcoma cell growth and lung metastasis by targeting Aurora-B. Cancer Manag. Res. *10*, 6305–6315.

21. Saleh, A.D., Savage, J.E., Cao, L., Soule, B.P., Ly, D., DeGraff, W., Harris, C.C., Mitchell, J.B., and Simone, N.L. (2011). Cellular stress induced alterations in microRNA let-7a and let-7b expression are dependent on p53. PLoS One *6*, e24429.

22. Marson, A., Levine, S.S., Cole, M.F., Frampton, G.M., Brambrink, T., Johnstone, S., Guenther, M.G., Johnston, W.K., Wernig, M., Newman, J., et al. (2008). Connecting microRNA genes to the core transcriptional regulatory circuitry of embryonic stem cells. Cell *134*, 521–533.

23. Pasquinelli, A.E., Reinhart, B.J., Slack, F., Martindale, M.Q., Kuroda, M.I., Maller, B., Hayward, D.C., Ball, E.E., Degnan, B., Müller, P., et al. (2000). Conservation of the sequence and temporal expression of let-7 heterochronic regulatory RNA. Nature *408*, 86–89.

24. Duldulao, M.P.N., Lee, W., Le, M., Chen, Z., Li, W., Kim, J., and Garcia-Aguilar, J. (2011). Let-7 microRNA regulates p53 and K-ras in colorectal cancer cells. J. Am. Coll. Surg. *213*, S25.

25. Johnson, S.M., Grosshans, H., Shingara, J., Byrom, M., Jarvis, R., Cheng, A., Labourier, E., Reinert, K.L., Brown, D., and Slack, F.J. (2005).

RAS is regulated by the let-7 microRNA family. Cell *120*, 635–647.

26. Johnson, C.D., Esquela-Kerscher, A., Stefani, G., Byrom, M., Kelnar, K., Ovcharenko, D., Wilson, M., Wang, X., Shelton, J., Shingara, J., et al. (2007). The let-7 microRNA represses cell proliferation pathways in human cells. Cancer Res. *67*, 7713–7722.

27. Schultz, J., Lorenz, P., Gross, G., Ibrahim, S., and Kunz, M. (2008). MicroRNA let-7b targets important cell cycle molecules in malignant melanoma cells and interferes with anchorage-independent growth. Cell Res. *18*, 549–557.

28. Alexandri, C., Stamatopoulos, B., Rothé, F., Bareche, Y., Devos, M., and Demeestere, I. (2019). MicroRNA profiling and identification of let-7a as a target to prevent chemotherapy-induced primordial follicles apoptosis in mouse ovaries. Sci. Rep. *9*, 9636.

29. Houbaviy, H.B., Murray, M.F., and Sharp, P.A. (2003). Embryonic stem cell-specific MicroRNAs. Dev. Cell *5*, 351–358.

30. Gonzales, K.A.U., Liang, H., Lim, Y.S., Chan, Y.S., Yeo, J.C., Tan, C.P., Gao, B., Le, B., Tan, Z.Y., Low, K.Y., et al. (2015). Deterministic Restriction on Pluripotent State Dissolution by Cell-Cycle Pathways. Cell *162*, 564–579.

31. Yuan, K., Ai, W.B., Wan, L.Y., Tan, X., and Wu, J.F. (2017). The miR-290-295 cluster as multi-faceted players in mouse embryonic stem cells. Cell Biosci. *7*, 38.

32. Imbalzano, A.N., and Jones, S.N. (2005). Snf5 tumor suppressor couples chromatin remodeling, checkpoint control, and chromosomal stability. Cancer Cell *7*, 294–295.

33. Langmead, B., Trapnell, C., Pop, M., and Salzberg, S.L. (2009). Ultrafast and memory-

efficient alignment of short DNA sequences to the human genome. Genome Biol. *10*, R25.

34. Enright, A.J., John, B., Gaul, U., Tuschl, T., Sander, C., and Marks, D.S. (2003). MicroRNA targets in Drosophila. Genome Biol. *5*, R1.

35. Friedländer, M.R., Mackowiak, S.D., Li, N., Chen, W., and Rajewsky, N. (2012). miRDeep2 accurately identifies known and hundreds of novel microRNA genes in seven animal clades. Nucleic Acids Res. *40*, 37–52.

36. Wen, M., Shen, Y., Shi, S., and Tang, T. (2012). miREvo: an integrative microRNA evolutionary analysis platform for next-generation sequencing experiments. BMC Bioinf. *13*, 140.

37. Anders, S., and Huber, W. (2010). Differential expression analysis for sequence count data. Genome Biol. *11*, R106.

38. Wang, L., Feng, Z., Wang, X., Wang, X., and Zhang, X. (2010). DEGseq: an R package for identifying differentially expressed genes from RNA-seq data. Bioinformatics *26*, 136–138.

39. Mao, X., Cai, T., Olyarchuk, J.G., and Wei, L. (2005). Automated genome annotation and pathway identification using the KEGG Orthology (KO) as a controlled vocabulary. Bioinformatics *21*, 3787–3793.

40. Ebert, M.S., Neilson, J.R., and Sharp, P.A. (2007). MicroRNA sponges: competitive inhibitors of small RNAs in mammalian cells. Nat. Methods *4*, 721–726.

41. Xi, J., Wu, Y., Li, G., Ma, L., Feng, K., Guo, X., Jia, W., Wang, G., Yang, G., Li, P., and Kang, J. (2017). Mir-29b Mediates the Neural Tube versus Neural Crest Fate Decision during Embryonic Stem Cell Neural Differentiation. Stem Cell Rep. *9*, 571–586.

STAR★METHODS

KEY RESOURCES TABLE

REAGENT or RESOURCE	SOURCE	IDENTIFIER
Chemicals, peptides, and recombinant proteins		
Feeder DMEM	Gibco	C11960500BT
Feeder FBS	Gibco	16000-044
Knockout DMEM	Gibco	10829-018
Knockout serum replacement	Gibco	10829-028
ESCs DMEM	Millipore	SLM-220-M
ESCs FBS	Thermo scientific	SH30070.03
L-Glutamine	Gibco	25030-081
Nucleosides	Millipore	ES-008-D
2-mercaptoethanol	Gibco	21985-023
NEAA	Millipore	TMS-001-C
Mouse Lif	Millipore	ESG1107
CHIR99021(GSK3 inhibitor)	Stemgent	04-0004
PD0325901(MEK inhibitor)	Stemgent	04-0006
Verapamil	Sigma	V4629
Hoechesst33342	Sigma	B2261
DPBS	Gibco	C14190500BT
TRIzol	Takara	9109
TE(0.05 % Trypsin-EDTA)	Gibco	25300054
Doxycycline hyclate	Merck	33429
Critical commercial assays		
Real-time qPCR kit SYBR Premix Ex TaqII	Takara	RR820A
All in one reverse transcription kit	Abm	G486
NucleoSpin Geland PCR Clean-up	MACHEREY-NAGEL	740609.250
EndoFree Plasmid Maxi Kit	QIAGEN	12362
Deposited data		
GSE252136	This study	N/A
Experimental models: Cell lines		
A129-2	He, W. et al. (2018)[11]	N/A
A129-6	This study	N/A
A129-17	This study	N/A
mRS	This study	N/A
Oligonucleotides		
Let-7a sponge-F	GCTAGCAACTATACAAGATCTACCTCACCGAACTATACA AGATCTACCTCAGCGAACTATACAAGATCTACCTCAGTCGAC	Plasmid construction
Let-7a sponge-R	GTCGACTGAGGTAGATCTTGTATAGTTCGCTGAGGTAG ATCTTGTATAGTTCGGTGAGGTAGATCTTGTATAGTTGCTAGC	Plasmid construction
Let-7a OE-F	GGAGAATTGGCTAGCCAGGTGTATCATATAATACA	Plasmid construction
Let-7a OE-R	GTCACTATGGTCGACATCATCATCAATCAAAATTA	Plasmid construction
Let-7g OE-F	GGAGAATTGGCTAGCTATATATAAATGACTGGTGT	Plasmid construction
Let-7g OE-F	GTCACTATGGTCGACTATATTCTGTAACAGTTTCA	Plasmid construction

(Continued on next page)

Continued

REAGENT or RESOURCE	SOURCE	IDENTIFIER
290-295 cluster family OE-F	GGAGAATTGGCTAGCAAGTGAGTAGTCTGGGCGCG	Plasmid construction
290-295cluster family OE-R	GTCACTATGGTCGACCAGTGATTAAAAGGGTGCTT	Plasmid construction
Let-7a sponge RT-F	GCTAGCAACTATACAAGATC	qRT-PCR
Let-7a sponge RT-R	GTCGACTGAGGTAGATCTTG	qRT-PCR
Let-7a OE-RT-F	TTCACTGTGGGATGAGGTAG	qRT-PCR
Let-7a OE-RT-R	ATCACCTTAGGAAAGACAGT	qRT-PCR
Let-7g OE-RT-F	CCAGGCTGAGGTAGTAGTTT	qRT-PCR
Let-7g OE-RT-R	CCTGGCAAGGCAGTGGCCTG	qRT-PCR
Bcl-2-F	GAACTGGGGGAGGATTGTGG	qRT-PCR
Bcl-2-R	GCATGCTGGGGCCATATAGT	qRT-PCR
Alk-F	TCTCCTGCATTGTGTCACCC	qRT-PCR
Alk-R	ATGGAGGAAGTCTTGCCAGC	qRT-PCR
Caspase 1-F	GGACCCTCAAGTTTTGCCCT	qRT-PCR
Caspase 1-R	GCAAGACGTGTACGAGTGGT	qRT-PCR
Caspase 2-F	CACACTACCAGCTGGCCTAT	qRT-PCR
Caspase 2-R	TGTGCGGTCTGGTCATGTAG	qRT-PCR
Caspase 3-F	GTCATCTCGCTCTGGTACGG	qRT-PCR
Caspase 3-R	CACACACACAAAGCTGCTCC	qRT-PCR
P16-F	CTTGGTGAAGTTCGTGCGAT	qRT-PCR
P16-R	AGAAGGTAGTGGGGTCCTCG	qRT-PCR
P53-F	CACCTCACTGCATGGACGAT	qRT-PCR
P53-R	GTGGAAGCCATAGTTGCCCT	qRT-PCR
Bax-F	CTCAAGGCCCTGTGCACTAA	qRT-PCR
Bax-R	GAGGCCTTCCCAGCCAC	qRT-PCR
Hras-F	CCTACCGGAAACAGGTGGTC	qRT-PCR
Hras-R	TTTCACCCGCTTGATCTGCT	qRT-PCR
Mcl1-F	GGGGCAGGATTGTGACTCTTA	qRT-PCR
Mcl1-R	GAACTCCACAAACCCATCCCAG	qRT-PCR
Survinvin-F	CTTCATCCACTGCCCTACCG	qRT-PCR
Survinvin-R	GTTGGTCTCCTTTGCAATTTTGT	qRT-PCR
Cdk1-F	ACACACGAGGTAGTGACGC	qRT-PCR
Cdk1-R	TCTGAGTCGCCGTGGAAAAG	qRT-PCR
Cdk2-F	CTGGGACTGCCGTGCTC	qRT-PCR
Cdk2-R	TTCAGTCTCAGTGTCGAGCC	qRT-PCR
Cdk4-F	TCGATATGAACCCGTGGCTG	qRT-PCR
Cdk4-R	CACAGACATCCATCAGCCGTA	qRT-PCR
Cdk6-F	CGCCTATGGGAAGGTGTTCA	qRT-PCR
Cdk6-R	GCACACATCAAACAACCTGACC	qRT-PCR
Cdc45-F	TCTAAGTATGCCAGGGTCAGA	qRT-PCR
Cdc45-R	CTGATTGGTTCCTTGTTGCCG	qRT-PCR
Cdc20-F	GCCCACCAAAAAGGAGCATC	qRT-PCR
Cdc20-R	GATTTCGGGGGCATCAAGGA	qRT-PCR
Wee1-F	ATTGGCTGGCTCTGTTGATGA	qRT-PCR
Wee1-R	CAGCTAAACTCCCACCATTACA	qRT-PCR
APC-F	GTCGGCTACCGTTGAGGAAG	qRT-PCR

Continued

REAGENT or RESOURCE	SOURCE	IDENTIFIER
APC-R	TTGGCTACCCTTGGACCTGC	qRT-PCR
E2F5-F	TCTCAAAGCGGCTGCAGATA	qRT-PCR
E2F5-F	TTACAGCCAGCACCTACACC	qRT-PCR
Ccnd1-F	TCAAGTGTGACCCGGACTG	qRT-PCR
Ccnd1-R	GCTCCTTCCTCTTTGCGGG	qRT-PCR
Chek2-F	GTCTCACGCGGTCGGATA	qRT-PCR
Chek2-R	GCAACTGAGAAGGAGTGCCT	qRT-PCR
Ccng2-F	CGACACGATGAAGGATTTGGG	qRT-PCR
Ccng2-R	AGCCTCCATCAAGATCAGCC	qRT-PCR
Ccnb1-F	ATAATCCCTCTCCAAGCCCGA	qRT-PCR
Ccnb1-R	TAACTGACTGCTCTTCCTCCAG	qRT-PCR
Bub3-F	CTTAGGCGGACAGGAGATGAC	qRT-PCR
Bub3-R	AGTGTGCTGGTACTTGAGCC	qRT-PCR
Bub1b-F	GCAGGCTGTTCAGCAAGAAG	qRT-PCR
Bub1b-R	ACTGGAACCTTTAGAATCAGGC	qRT-PCR
Oct4-RT-F	CTGAGGGCCAGGCAGGAGCACGAG	qRT-PCR
Oct4-RT-R	CTGTAGGGAGGGCTTCGGGCACTT	qRT-PCR
Klf4-RT-F	CACCATGGACCCGGGCGTGGCTGCCAGAAA	qRT-PCR
Klf4-RT-R	TTAGGCTGTTCTTTTCCGGGGCCACGA	qRT-PCR
Nanog-RT-F	CGGTTCATCATGGTACAGTC	qRT-PCR
Nanog-RT-R	CAGGTGTTTGAGGGTAGCTC	qRT-PCR
Sox2-RT-F	TTGCCTTAAACAAGACCACGAAA	qRT-PCR
Sox2-RT-R	TAGAGCTAGACTCCGGGCGATGA	qRT-PCR
Myc-F	GTTGGAAACCCCGCAGACA	qRT-PCR
Myc-R	CCAGATATCCTCACTGGGCG	qRT-PCR
Esrrb-RT-F	GAACAGCCCCTACCTGAACC	qRT-PCR
Esrrb-RT-R	ATGAGGAACACAAGCTCCCG	qRT-PCR
Software and algorithms		
Graphpad prism 8	Graphpad	N/A
Bowtie-0.12.9	https://sourceforge.net/projects/bowtie-bio/files/bowtie/0.12.9/	N/A
miREvo_1.1	https://github.com/akahanaton/miREvo	N/A
Mirdeep2_0_0_5	https://github.com/rajewsky-lab/mirdeep2	N/A
repeatmasker	https://www.repeatmasker.org/RepeatMasker/	N/A
miRanda-3.3a	https://bioweb.pasteur.fr/packages/pack@miRanda@3.3a	N/A
psRobot_V1.2	http://omicslab.genetics.ac.cn/psRobot/	N/A
DEseq2	https://bioconductor.org/packages/release/bioc/html/DESeq2.html	N/A
DEGSeq	https://bioconductor.org/packages/release/bioc/html/DEGseq.html	N/A
KOBAS 2.0	http://bioinfo.org/kobas	N/A

RESOURCE AVAILABILITY

Lead contact

Further information and requests for resources and reagents should be directed to and will be fulfilled by the lead authors, Zhiming Han (hanzm@ioz.ac.cn).

Materials availability

This study did not generate new unique reagents.

Data and code availability

The raw sequence data have been uploaded to GEO datasets. These data can be obtained from the GEO database (GSE252136 dataset).

This paper does not report original code.

The data that support the findings of this study are available upon request from the corresponding authors.

EXPERIMENTAL MODEL AND STUDY PARTICIPANT DETAILS

Mice

The 129Sv mice used in the experiments were housed in the specific-pathogen-free-grade animal facility and all animal experiments were approved by the Biological Research Ethics Committee of Tongji University and the Animal Research Committee of the Institute of Zoology, Chinese Academy of Sciences.

METHOD DETAILS

Derivation and maintenance of mAG-haESCs

mAG-haESC derivation and culture were conducted as previously described.[11] Briefly, all mAG-haESCs were derived in 15% KSR knockout DMEM (Gibco) supplemented with 0.1 mM mercaptoethanol (Merck Millipore), 1 mM L-glutamine (Merck Millipore), nucleosides (100×, Merck Millipore), 1% nonessential amino acid stock (Merck Millipore), penicillin/streptomycin (100×, Merck Millipore), 2i (1 μM PD0325901 and 3 μM CHIR99021), and 1,000 U/mL mouse LIF (Merck Millipore). Haploid cells were sorted after outgrowth cells expanded to one 12-well plate. Then, mAG-haESCs were propagated in 15% FBS ES medium supplemented with 1 mM L-glutamine, 0.1 mM mercaptoethanol, nucleosides (100×), 1% nonessential amino acid stock, penicillin/streptomycin (100×), 2i, and 1,000 U/mL mouse LIF. Periodic enrichment (every 3∼5 weeks, depending on the cell lines) of haploid cells treated with staining buffer (15 μg/mL Hoechst 33342 and 2.5 μM verapamil) was conducted with a BD FACS Aria II cell sorter.

Collection of mRS, mAG-haESCs and R1 cells

Haploid germ cells were collected from the testes of male 129Sv mice. The testes were collected with scissors, and the surrounding fatty tissue was removed. After opening the testicular capsule under a microscope, the seminiferous tubules were released and placed into a 1.5 mL Eppendorf tube. After the seminiferous tubules were cut with scissors for 1 min, 400 μL of 0.05% trypsin-EDTA was added, and the tissue was digested for 4 min and then neutralized with 600 μL of feeder medium. Germ cells were filtered through a 70 μm filter and then centrifuged at 1000 rpm for 5 minutes. Then, germ cells were stained with Hoechst 33342 at 37°C for 30 minutes, centrifuged and resuspended in FACS buffer. Finally, mRS cells were sorted with a BD FACSAria II cell sorter after filtration through a 40 μm filter.

mRS, mAG-haESCs and R1 cells were collected in 15 ml tubes with 1 ml of DPBS. Cell sorting was completed in 2 hr to avoid cell death. Samples of more than 5×10⁶ cells from each mAG-haESC line, R1 and mRS were collected in 2-3 independent replicates by FACS sorting. Samples were lysed in TRIzol to isolate sRNAs after centrifugation at 1400 rpm for 5 min to remove the cell culture medium (supernatant).

sRNA extraction

RNA was extracted using a QIAGEN RNA kit or off-site at Novogene (for sRNA extraction). The quality of the sRNAs was checked prior to library construction by 1% agarose gels and RNA integrity was checked by NanoPhotometer® spectrophotometer, and samples of sRNAs without degradation and genomic DNA contamination were considered appropriate for use.

sRNA library construction and sequencing

Three micrograms of total RNA from each sample were used for library construction with the NEBNext® Multiplex Small RNA Library Prep Set for Illumina® (NEB, USA). Briefly, the 3' adapter was first ligated to the sRNAs, followed by ligation of the 5' adapter. Then, the ligation-reconstructed sRNAs were reverse transcribed into small cDNAs. After amplification by PCR, a library with a length of 140∼160 bp was purified by gel excision. Library quality was checked on an Agilent Bioanalyzer 2100 system before sequencing. sRNA sequencing was conducted on the NovaSeq 6000 SE50 platform, and at least 10 M clean reads were obtained for each sample.

sRNA data analysis

Bowtie-0.12.9 was used to map sRNA tags to the reference sequence;[33] miRanda-3.3a was used to predict miRNA target genes,[34] and known miRNA analysis was performed by miRDeep2 (mirdeep2_0_0_5).[35] miRDeep2 and miREvo were used for novel miRNA prediction.[36] Biological repeat analysis was performed with DEseq2 (1.12.0) (padj<0.05),[37] and DEGseq (1.2.2) was used to analyze nonrepeats (q value<0.01, |log2-foldchange|>1).[38] The enrichment of target gene candidates in pathways was determined via KOBAS (V2.0) (blastx 1e-10; p.adjust:BH).[39]

The piRBase and piRNA bank databases were used for piRNA annotation. For sRNA mapping to biotype annotation, we followed the priority rule: known miRNA > rRNA > tRNA > piRNA >snRNA > snoRNA > repeat > gene > novel miRNA.

Quality control of the sRNA sequencing data

To ensure good accuracy of the sequencing data, the sequencing error rate of each base position was less than 0.5%, and the GC content was approximately 50%. To ensure the quality of the information analysis, the raw reads that contained low-quality reads or adapter sequences were eliminated to obtain clean reads. Each sample yielded more than 90% clean reads.

Design and construction of miRNA sponges

miRNA sponges were designed following a previous report.[40,41] Then, 3 tandemly repeated miRNA sponges were constructed in the PCW57.1 plasmid, which is under the control of Dox induction. The reconstructed plasmid was packaged in lentivirus and transfected into mAG-haESCs. After selection with puromycin for one week, the A129-2-let-7 sponge cell line was established.

Transfection of miRNA into mAG-haESCs

miRNA mimics and inhibitors were synthesized by GenePharma and transfected into mAG-haESCs by using Lipo2000. Briefly, 6 μL of Lipo2000 was added to 400 μL of Opti-MEM, while 10 μL of mimic/inhibitor (20 μM) was added to 400 μL of Opti-MEM. After the mixture was allowed to stand at room temperature for 5 minutes, diluted Lipo2000 was added to the diluted mimics/inhibitor, mixed thoroughly, and allowed to stand at room temperature for 15 minutes. The mixture was added to a 12-well plate of mAG-haESCs at the proper density.

QUANTIFICATION AND STATISTICAL ANALYSIS

Unless otherwise stated in the figure legends, all the date were analyzed by using GraphPad Prism (9.0.0) software. The data are presented as the mean $\pm$ SEM from at least three independent experiments. *$p < 0.05$; **$p < 0.01$; ***$p < 0.001$; ****$p < 0.0001$ by Student's t test for comparison.